Tellus (2007), 59A, 336–343
Printed in Singapore. All rights reserved

TELLUS

Improved simulation of water vapour and clear-sky radiation using 24-hour forecasts from ERA40

By RICHARD P. ALLAN*, *ESSC, University of Reading, Reading, RG6 6AL, United Kingdom*

(Manuscript received 22 August 2006; in final form 8 January 2007)

ABSTRACT

Monthly mean water vapour and clear-sky radiation extracted from the European Centre for Medium Range Weather Forecasts 40-year reanalysis (ERA40) forecasts are assessed using satellite observations and additional reanalysis data. There is a marked improvement in the interannual variability of column-integrated water vapour (CWV) over the oceans when using the 24-hour forecasts compared with the standard 6-hour forecasts products. The spatial distribution of CWV are well simulated by the 6-hour forecasts; using the 24-hour forecasts does not degrade this simulation substantially and in many cases improves on the quality. There is also an improved simulation of clear-sky radiation from the 24-hour forecasts compared with the 6-hour forecasts based on comparison with satellite observations and empirical estimates. Further work is required to assess the quality of water vapour simulation by reanalyses over land regions. Over the oceans, it is recommended that 24-hour forecasts of CWV and clear-sky radiation are used in preference to the standard 6-hour forecast products from ERA40.

1. Introduction

Tropospheric water vapour and clear-sky radiative cooling are important components of the atmospheric hydrological cycle (e.g. Stephens et al., 1994). Accurate representation of these quantities is critical for climate prediction, and therefore model simulation of these diagnostics must be continually evaluated. Satellite measurements and ground-based observations offer a powerful means of assessing model skill. However, where observational sampling is limited, reanalyses present an additional powerful source of information on the state of the atmosphere.

Previously, it has been shown that the European Centre for Medium Range Weather Forecasts 40-year reanalysis (ERA40) provides an accurate spatial representation of water vapour and clear-sky radiation but that interannual variability is poor (Allan et al., 2004; Trenberth et al., 2005). Recently, Uppala et al., (2005) showed an improved representation of column-integrated water vapour (CWV) and precipitation simulated by 24-hour forecasts from ERA40 compared with the standard 6-hourly analysis products over the tropical oceans. The present study seeks to assess in more detail the global performance of the 24-hour forecasts. In particular, does the improved simulation of water vapour variability compromise the high-quality spatial variability in water vapour and clear-sky radiation simulated by ERA40?

*Correspondence.
e-mail: rpa@mail.nerc-essc.ac.uk
DOI: 10.1111/j.1600-0870.2007.00229.x

2. Data

Monthly-mean CWV, clear-sky outgoing long-wave radiation (OLRc) and surface net long-wave radiation (SNLc) from ERA40 are sampled on a 2.5° × 2.5° spatial grid over the period 1979–2001. The 6-hour and 24-hour forecasts are used to generate CWV while the clear-sky radiation diagnostics are available as accumulations over 0–6 hours and 24–36 hours.

In addition to ERA40, data from the National Center for Environmental Prediction/National Center for Atmospheric Research reanalysis 1 (NCEP; Kalnay et al., 1996) for 1979–2004 on a 1.875° longitude by 1.9° latitude spatial grid were acquired. Allan et al. (2004) found that the spatial distribution of water vapour and clear-sky radiation in NCEP showed poorer agreement with observations compared with ERA40 but the accuracy of interannual anomalies was superior in NCEP (see also Yang et al., 1999).

Release 2 of the Surface Radiation Budget (SRB; Stackhouse et al., 1999) project provided clear-sky fluxes on a 1° × 1° spatial grid from 1983–1994; the clear-sky SRB fluxes are determined primarily by reanalysis data. Comparisons with ground-based observations suggest an rms bias error of 13.5 Wm^{-2} in all-sky longwave fluxes (for details see http://eosweb.larc.nasa.gov/).

Observations of CWV over the ice-free ocean were provided by the Scanning Multichannel Microwave Radiometer (SMMR; Wentz and Francis, 1992) for the period 1979–1984 and from version 5 of the Special Sensor Microwave Imager (SSM/I; Wentz, 1997) for the period 1987–2004. The SMMR data were bilinearly interpolated from a 1° × 1° resolution to the ERA40 grid.

SSM/I data were provided on a 0.25° × 0.25° grid and averaged up to the ERA40 grid only where the 2.5° × 2.5° grid-box contained more than 70% data coverage. An expected rms calibration error of 1.2 mm applies for the SSM/I data (Wentz, 1997).

The SMMR and SSM/I data were also used as input to an empirical formula (Prata, 1996) to provide an observationally derived estimate of SNLc variability. Calculations were conducted on a 1° × 1° resolution grid using also sea surface temperature data from the Hadley Centre global sea Ice and Sea Surface Temperature dataset (HadISST; Rayner et al., 2003) and a sea surface minus air temperature climatology from da Silva et al. (1994); for further details, see Allan (2006).

Finally, satellite observations of OLRc were used from multiple platforms: the Earth Radiation Budget Satellite (ERBS; 1985–1989), the Scanner for Radiation Budget instrument (ScaRaB; 1994–1995), and the Clouds and the Earth's Radiant Energy System (CERES) instruments (version ES4_TRMM-PFM_EDITION2_015013 for 1998 and version ES4_Terra-FM1_Edition2_024026 for 2000–2004). These data are described in Wielicki et al. (2002) and references therein; an absolute calibration uncertainty of 1% and 0.5% applies to the pre-CERES and CERES instruments, which translates to an approximate calibration uncertainty in low-latitude clear-sky OLR of 2.5 and 1.5 Wm^{-2}, respectively. Additional factors, including sampling of clear skies, will increase these uncertainties further.

3. Column-integrated water vapour

Uppala et al. (2005) demonstrated an improved simulation of CWV over the tropical oceans in the 24-hour forecasts from ERA40 compared to the 6-hour forecasts. Figure 1 confirms this for a larger domain (40°S-40°N). Overestimates by the 6-hour forecasts of order 1 mm (∼3%) compared with the satellite observations are evident for the periods 1982–1983 and 1989–2001; these discrepancies are substantially reduced using the 24-hour forecasts. Both ERA40 products simulate lower CWV than SMMR in 1984 and SSM/I during 1987 with the differences being slightly larger for the 24-hour forecasts. While the NCEP data accurately reproduce the observed interannual variability in CWV, as quantified by the standard deviation (Table 1), the mean is about 3% lower than the satellite measurements for the low-latitude ocean. This may relate to the unrealistic spatial representation of water vapour provided by NCEP (Allan et al., 2004). The correlation between all reanalysis products and SSM/I is significant at the 95% level allowing for autocorrelation of the data using the method of Yang and Tung (1998) with the ERA40 24-hour forecasts giving the highest correlation coefficient of 0.86 (Table 1).

Table 1. Variability in monthly-mean water vapour and de-seasonalised monthly-mean clear-sky radiation anomalies and correlation with observed and empirical estimates over low-latitude oceans (40°S–40°*N*). OBS denotes SSM/I data for CWV (1988–2001), empirical estimates of SNLc derived from SSM/I and other data (1988–2001) and ERBS OLRc observations over the period 1985–89. An asterisk denotes significant correlation at the 95% level allowing for autocorrelation of the data

Parameter	ERA40 6-hour	ERA40 24-hour	NCEP	OBS
Standard Deviation				
CWV (mm)	0.85	0.69	0.60	0.62
SNLc (Wm^{-2})	0.87	0.73	0.65	0.42
OLRc (Wm^{-2})	0.71	0.70	0.42	0.40
Correlation (*r*)				
CWV	0.78*	0.86*	0.73*	
SNLc	0.69	0.77	0.69	
OLRc	0.32	0.42	0.59	

The time-series analysis above was also repeated for the 50°S–50°N region (not shown). This gave similar results to Fig. 1 but with poorer agreement between ERA40 and SMMR data, explained in part by the increased occurrence of missing satellite data at higher latitudes. The effect of the missing data on these comparisons was investigated further by performing an alternative averaging strategy. Rather than calculating an area-weighted average of all non-missing oceanic data as in Fig. 1, ocean-means were also calculated by first computing zonal means from the non-missing data and subsequently performing an area-weighted average of the zonal means for each dataset (not shown). While the differing methods alter the seasonal variability substantially, the interannual anomalies (calculated by removing the mean seasonal cycle) and the inter-dataset differences are not strongly affected. For the SMMR and SSM/I data, the different averaging methods cause differences in the interannual anomalies of less than 0.13 mm (∼0.4%) for all but November–December

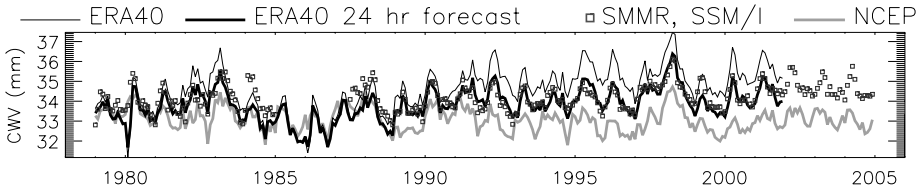

Fig. 1. Time series of monthly-mean column integrated water vapour (CWV) over the oceans (40°S–40°N).

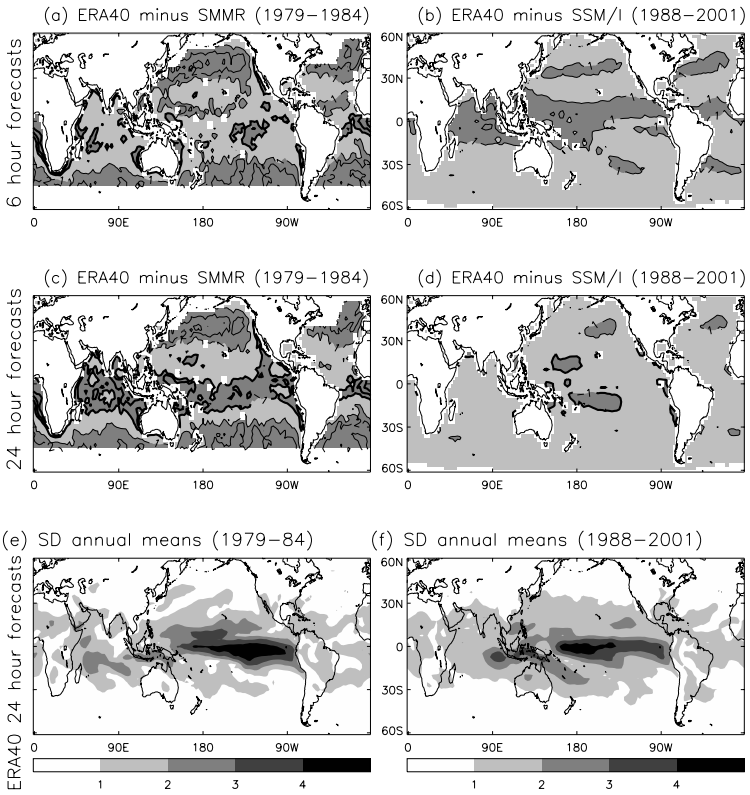

Fig. 2. Differences in column-integrated water vapour (CWV) over the ocean: ERA40 6-hour forecasts minus (a) SMMR for 1979–1984 and (b) SSM/I for 1988–2001 and ERA40 24-hour forecasts minus (c) SMMR and (d) SSM/I. Dark shading denotes differences larger in magnitude than 1 mm; negative differences have thick contours. The standard deviation of annual mean CWV from the ERA40 24-hour forecasts are presented for the period (e) 1979–1984 and (f) 1988–2001.

1982 and December 1987, due to increased quantities of missing data, where differences were still below 1% of the mean CWV.

While the 24-hour forecast data from ERA40 substantially improve the simulated variability in water vapour, it is important to demonstrate that these products maintain the robust spatial structure in humidity fields displayed by the 6-hour forecast products. Figure 2 shows differences in CWV (ERA40 minus satellite data) for the 6-hour and 24-hour forecasts. For both products, differences are larger for comparisons with the SMMR data compared to the ERA40 minus SSM/I differences which are generally smaller than 2 mm. This is unsurprising since SSM/I radiance data is assimilated by ERA40. The 6-hour forecasts overestimate CWV over mid-latitudes by ∼2 mm and underestimate by a smaller magnitude over equatorial regions compared to SMMR (Fig. 2a). Similar results are found for the 24-hour forecasts (Fig. 2c), apart from over equatorial regions where the negative bias becomes more widespread.

The ERA40 6-hour forecasts overestimate CWV by about 1–2 mm over the tropics compared with SSM/I (Fig. 2b). The 24-hour forecasts underestimate CWV over the same region but by a smaller magnitude (Fig. 2d). Over the vast majority of the ice-free oceans, the 24-hour forecasts from ERA40 reproduce the SSM/I observations to within the expected rms inter-calibration error of 1.2 mm (Wentz, 1997) and are substantially smaller than the interannual standard deviation of CWV over much of the tropical ocean (Fig. 2e and f). In summary, the high-quality simulation of CWV distribution provided by ERA40 6-hour forecasts are maintained and in some cases improved by using the 24-hour forecasts with the possible exception of the equatorial belt for the 1979–1984 comparisons. Combined with the improved representation of interannual variability, the 24-hour forecasts of CWV are indeed superior in quality to the 6-hour forecasts as indicated by Uppala et al. (2005).

4. Clear-sky radiation

The improved simulation of water vapour suggests that a more robust representation of clear-sky radiation may also be attained by using the 24–36 hour forecast accumulations from ERA40.

4.1. Clear-sky surface net long-wave radiation

The upwelling and downwelling surface long-wave fluxes are influenced primarily by surface skin and near-surface temperature and CWV for clear-sky conditions (e.g., Prata, 1996). Over land, large errors in surface skin temperature in the reanalysis will impact the quality of the upward long-wave flux at the surface. Nevertheless, since near-surface temperature is strongly coupled to surface skin temperature, the errors in upward and downward long-wave fluxes will compensate to a certain extent. For the net long-wave flux over low-latitude oceans, much of the long-wave spectrum is saturated by water vapour absorption/emission, and the net flux is strongly determined by CWV emission in the atmospheric window (e.g., Allan, 2006).

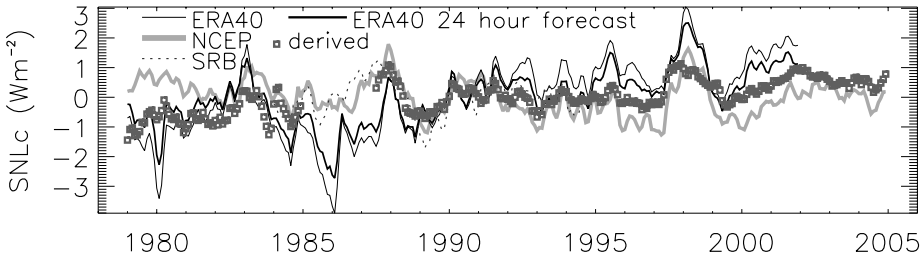

Fig. 3. De-seasonalised monthly-mean anomaly time series of clear-sky surface net long-wave radiative flux to the ocean (40°S–40°N). A 3-month running-mean was applied.

Therefore, it is reasonable to expect that improvements in CWV over the ocean in the 24-hour forecasts of ERA40 will also be detected in the simulations of clear-sky surface net long-wave radiation (SNLc).

Figure 3 displays time series of SNLc over the low-latitude oceans. The mean SNLc over this domain is approximately −70 to −80 Wm^{-2} (a surface cooling); thus, positive SNLc anomalies signify a heating of the surface (or a reduction in net cooling). The large seasonal cycle is calculated separately for each dataset and removed from the series and a 3-month running mean applied to highlight interannual anomalies. In addition to the ERA40 forecasts and NCEP data, also shown are data from SRB and empirically derived from the combination of SMMR-SSM/I, HadISST, and da Silva (Allan, 2006).

All datasets reproduce an increase in SNLc anomalies (surface heating) during the El Niño warm events of 1982–1983, 1986–1987, and 1997–1998. However, the nature of interannual variability varies substantially between dataset, possibly with the exception of the period 1988–1991 in which there is agreement to within about 0.5 Wm^{-2}. All reanalysis datasets overestimate the variability of SNLc compared to the empirical estimate, based on the standard deviation of the interannual anomalies (Table 1). Since the empirical estimate only accounts for the water vapour-related effect on variability, it is possible that the actual variability is somewhat larger. Nevertheless, the 24–36-hour forecast interannual standard deviation show better agreement and higher correlation with the empirical estimate than the 0–6-hour forecasts (Table 1).

The strongly negative SNLc anomalies for ERA40 during 1985–1987 are at odds with SRB and NCEP; these anomalies are smaller for the 24-hour forecast than the 6-hour forecasts. The predominantly negative SNLc anomalies before 1988 and positive anomalies after 1991 for ERA40 are reduced when comparing the 24-hour forecasts with 6-hour forecasts from ERA40; this effectively reduces the positive SNLc heating trend in ERA40 and improves agreement with the empirically derived variability. The derived estimate produces a positive SNLc trend (surface heating) over the period 1979–2004, in contrast to the NCEP data. The ERA40 and NCEP data both simulate a large increase in SNLc during 1997 of about 2–3 Wm^{-2} which is approximately double the response derived empirically.

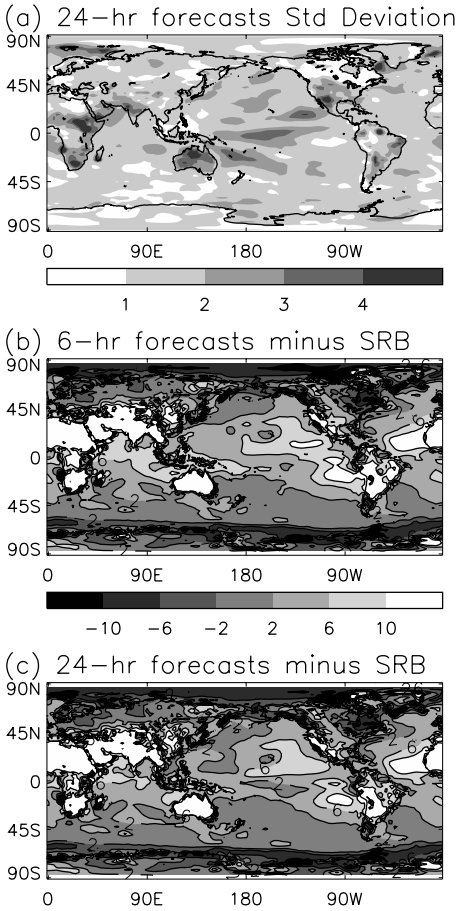

Fig. 4. (a) Standard deviation of annual mean SNLc from the ERA40 24–36-hour accumulations and the ERA-40 minus SRB differences over the period 1984–1994 for (b) ERA40 0–6-hour forecasts and (c) ERA40 24–36-hour forecasts (units: Wm^{-2})

The 0–6-hour and 24–36-hour SNLc forecasts both produce positive ERA40 minus SRB differences greater than 10 Wm^{-2} over Africa, India, Australia, Peru and also parts of the south-east Pacific and north-equatorial Atlantic (Fig. 4). Differences are larger than the interannual standard deviation (Fig. 4a) but smaller than the expected rms error associated with SRB all-sky long-wave fluxes.

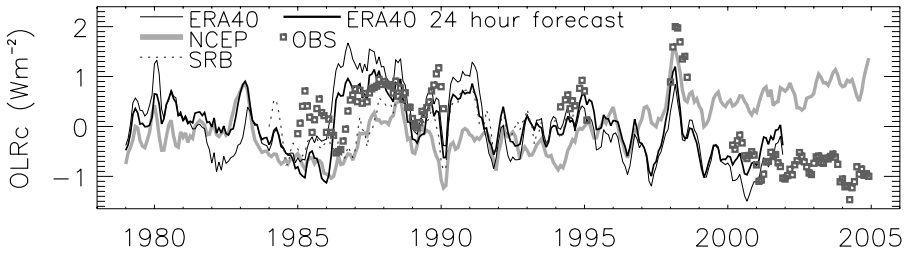

Fig. 5. De-seasonalised monthly-mean anomaly time series of clear-sky outgoing longwave radiation (OLRc) for the 40°S–40°N ocean region. A 3-month running-mean was applied.

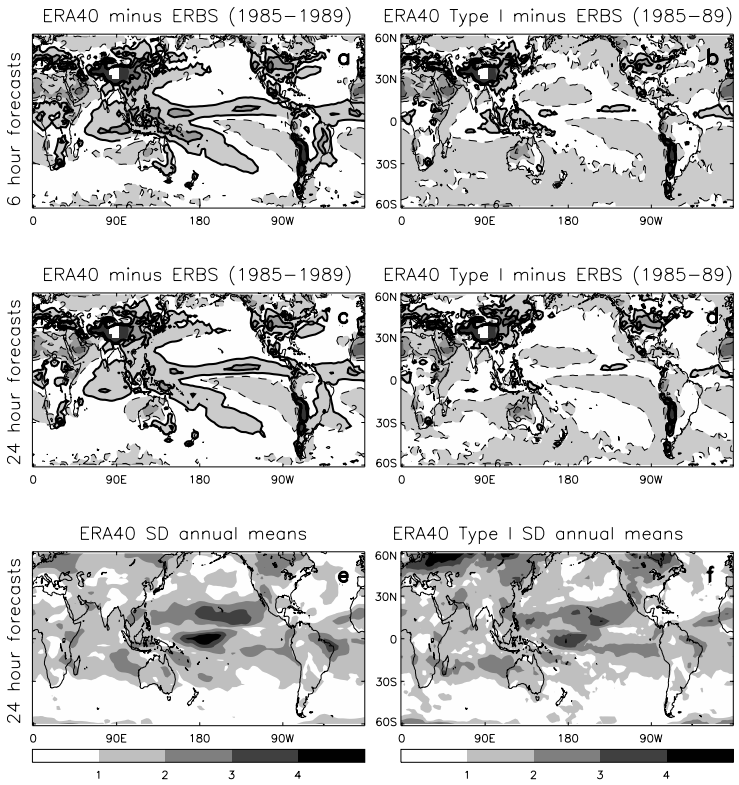

Fig. 6. ERA40 minus ERBS clear-sky outgoing long-wave radiation (OLRc) differences 1985–1989 for (a) ERA40 0–6-hour forecast, (b) ERA40 0–6-hour forecast satellite-like sampling, (c) ERA40 24–36-hour forecast and (d) ERA40 24–36-hour forecast satellite-like sampling. Shading denotes differences greater in magnitude than 2 Wm^{-2}; contours are for every 4 Wm^{-2} with solid contours for negative differences and dashed contours for positive differences. The standard deviation of annual mean OLRc from the ERA40 24–36-hour forecasts are presented for (e) standard accumulations and (f) modified satellite-like sampling diagniostics.

In summary, it is judged that the distribution of SNLc simulated by the 24–36-hour accumulations from ERA40 are similar in quality to the 6-hour forecasts while the 24–36-hour forecasts represent an improved interannual variability. Further comparisons with surface observations are required to demonstrate the robust nature of interannual variability in SNLc.

4.2. Clear-sky outgoing longwave radiation

Time series of OLRc over low-latitude oceans are presented in Fig. 5. Again, the mean seasonal cycle is removed from each dataset and a 3-month running mean applied. Despite significant satellite calibration uncertainty, changes in clear-sky sampling due to variable footprint size and variable spatio-temporal sampling, there is a good agreement between OLRc anomalies from ERA40 data and the observations, with the possible exception of 1985–1986, as found by Allan (2006). Notably, the observed drop in OLRc of about 2 Wm^{-2} from 1998 to 2000 is well captured by ERA40 but not by NCEP. The observed decreasing OLRc trend from 2000–2004 is not captured by ERA40 or NCEP. However, the observed trend is thought to be a calibration error that affects daytime long-wave fluxes in the Edition 2 Terra CERES data (Grant Matthews, pers. comm.). The 24–36-hour forecasts from ERA40 improve agreement with the other datasets compared with the 0–6-hour forecast, in particular with the satellite data over the period 1986–1989 and also for the period 1979–1983 in comparison with NCEP, including the simulation of the 1982–1983 El Niño warm event. Correlation with the ERBS observations is improved slightly by moving from 0–6 to 24–36-hour forecasts although the interannual variability is mostly unchanged and almost double the variability (quantified by the standard deviation) estimated by NCEP and ERBS (Table 1).

Differences between ERA40 and ERBS over the period 1985–1989 are presented in Fig. 6. In addition to the standard

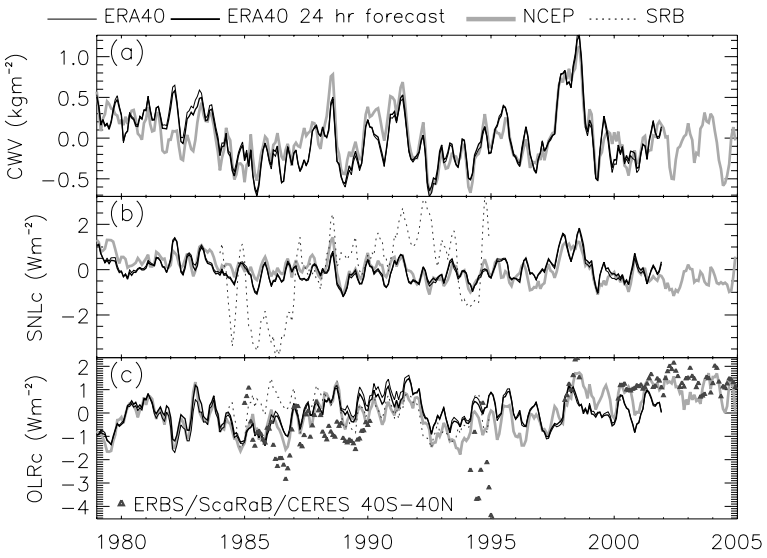

Fig. 7. Changes in water vapour and clear-sky radiation over land: (a) column-integrated water vapour, (b) clear-sky surface net downward longwave radiation, (c) clear-sky outgoing longwave radiation. The mean seasonal cycle is removed from each time-series and a 3-month running-mean applied.

clear-sky diagnostics, modified OLRc diagnostics (OLR_{cI}) were also calculated from the 6-hourly or 12-hourly accumulations over the period 1985–1989; these give greater weighting to cloud-free periods during a month and thereby mimic satellite sampling which only measures emitted radiation from cloud-free regions (e.g., Allan et al., 2003):

$$\mathrm{OLR}_{cI} = \frac{1}{n}\sum_{h=1}^{n}\frac{\sum_{d=1}^{N}\mathrm{OLR}c(1-Ac)}{\sum_{d=1}^{N}(1-Ac)}, \qquad (1)$$

where h is the hour interval (four 6-hour accumulations per day for the 6-hour forecast or two 12-hour accumulations per day for the 24–36-hour forecasts), d is the day of the month and Ac is the cloud fraction. The standard deviation of annual mean ERA40 data are also presented for the standard and Type I diagnostic in Figs. 6e and 6f.

As found by Allan et al. (2004), ERA40 6-hour forecasts simulate OLRc about 6 Wm^{-2} lower than ERBS over the tropical convective regimes (Fig. 6a). Much of this negative bias was explained by the disparate sampling of clear skies between the satellite and reanalysis data (Allan and Ringer, 2003); indeed, when the ERA40 data are sampled so as to give greater weighting to periods of lower cloud fraction, thereby mimicking satellite sampling, these negative differences mostly disappear and a residual positive ERA40 bias is apparent over much of the mid-latitude and convectively suppressed subtropical oceans (Fig. 6b). Similar results are found for the 24–36-hour forecasts from ERA40 (Figs. 6c and 6d), although differences are generally smaller than for the 6-hour forecast, albeit of the order of the satellite calibration uncertainty and the standard deviation of the annual means (Figs. 6e and 6f). The standard deviation of Type I diagnostics are slightly smaller than the standard diagnostics over the central Pacific since the modified clear-sky diagnostics sample a smaller subset of atmospheric conditions. Since the simulation of OLRc distribution by ERA40 is considered robust (Allan and Ringer, 2003), and the 24–36-hour forecasts appear to provide still better spatial and temporal comparisons with satellite datasets, these products are well suited to the evaluation of climate models (e.g., Huang et al., 2006).

5. Changes in water vapour and clear-sky radiation over land

Since satellite microwave observations of water vapour are only available over the ice-free oceans, evaluation of water vapour over land in reanalyses has been less extensive. Anomaly time series of water vapour and clear-sky radiation are now presented in Fig. 7. It is immediately apparent that agreement between ERA40 and NCEP simulations of CWV and clear-sky radiation is good, in contrast to the oceanic comparisons, in particular for CWV and SNLc. Further, the differences between the 0-6 hour and 24–36-hour simulations from ERA40 are small. These findings suggesting that the spurious water vapour and clear-sky radiation changes in ERA40 are confined to the oceans.

The simulation of SNLc anomalies by SRB contrasts markedly with ERA40 and NCEP (Fig. 7b); this is explained by the likely overestimation of land-surface temperature prior to 1987 which causes negative downward minus upward surface longwave anomalies, also evident in Fig. 4. An overestimation of SRB land surface temperature is also consistent with an overestimation in OLRc anomalies during this period compared with the other datasets considered (Fig. 7c). Agreement between ERA40 OLRc and the satellite observations is less good than over oceans, in particular for the beginning of 1985, and during 1994–1995 where the ScaRaB data indicates strongly negative anomalies compared to the ERBS and CERES data. Nevertheless, for the remaining periods of overlap with satellite data, anomalies are within the satellite calibration uncertainty of ∼1% (Wielicki et al., 2002). It is interesting to note that the large drop in oceanic OLRc from 1998–2000 seen in the CERES

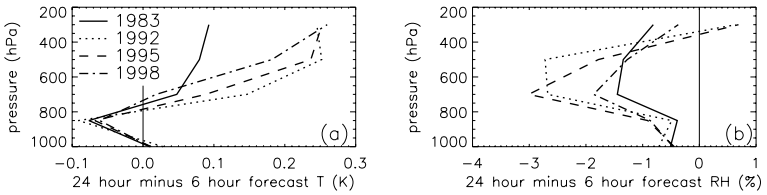

Fig. 8. Changes in April mean (a) temperature (K) and (b) relative humidity (%) for 24-hour minus 6-hour forecasts from ERA40 for 1983, 1992, 1995, and 1998.

and ERA40 data is not apparent over land for either dataset; this merits further analysis.

6. Discussion

The fact that the ERA40 24-hour forecasts show improvements compared to 6-hour forecasts over the ocean but not land suggests an assimilation issue with satellite water vapour channels. Uppala et al. (2005) related the unrealistic hydrological cycle in ERA40 to a combination of dry climatological bias in the model and the assimilation of erroneous information from satellite data. Figure 8 shows the April monthly-mean differences in temperature and relative humidity over the low-latitude ocean (40°S–40°N) at a number of pressure levels for the 24-hour minus 6-hour forecasts for 1983, 1992, 1995, and 1998. These months coincide with large changes in CWV between the 24-hour and 6-hour forecasts (Fig. 1). All months show decreases in temperature of up to 0.1 K around 850 hPa. A larger magnitude warming is evident in the upper troposphere, of up to 0.25 K, which is most pronounced in the tropics over the central Pacific and Indian Ocean (not shown). Relative humidity diminishes by around 1–3% in the mid-troposphere, originating primarily from the moist, tropical zone.

Since the background forecasts in ERA40 are systematically dry, and background errors in temperature are generally low, where problems arose in the availability and calibration of satellite channels, in particular data from the High-resolution Infra-Red Sounder (HIRS), there was a tendency for these errors to cause a perturbation in humidity (Uppala et al., 2005). This is apparent in Fig. 8 which shows relatively small changes in temperature compared to the large reduction in relative humidity for pressures greater than 400 hPa. The increase in humidity over moist regions resulted in unrealistically high precipitation and associated latent heat release, explaining the rise in upper tropospheric temperatures in the 24-hour forecasts. The reduction in humidity for the 400–800 hPa layers may also have cooled the 850 hPa level through increased long-wave radiative cooling to the upper troposphere. Since the initial errors in humidity were positive, the tendency toward a drier climatology resulted in better agreement with observations of CWV by the 24-hour forecasts. This is somewhat fortuitous since at longer forecast lead times, the model will subtend toward an unrealistically dry climatology.

The years 1983 and 1992 were problematic since stratospheric aerosol from the El Chichon and Pinatubo volcanic eruptions were not adequately corrected for in the HIRS retrievals. Improvements in the assimilation of HIRS channels were applied to years after 1997 and years before 1989; the temperature and humidity changes in 1983 are indeed smaller than 1992 (Fig. 8) although El Chichon ejected a smaller quantity of particulate matter into the stratosphere. The improvements in assimilation after 1997 also appear to reduce the model drying compared to 1992 and 1995 but a substantial drop in relative humidity of up to 2% is still present for April 1998, which occurred mainly along the inter-tropical convergence zone, suggesting that problems remain.

7. Conclusions

It has previously been reported that changes in the observing systems used in the current generation of reanalysis datasets, such as ERA40, contribute to spurious variability in the atmospheric hydrological cycle (Trenberth et al., 2005). Recently, Uppala et al. (2005) showed an improved representation in tropical water vapour variability in ERA40 when moving from the standard 6-hour forecast products to the 24-hour forecasts. Motivated by these results, the present study establishes that the improved water vapour variability in ERA40 24-hour forecasts applies to a much larger region of the global oceans. Importantly, the improved representation of ocean variability in water vapour does not compromise the high-quality simulation of the distribution of water vapour geographically and also contributes to the improved simulation of clear-sky radiation in the 24-hour forecasts relative to the standard ERA40 products. The global and low-latitude ocean mean values from ERA40 and NCEP are presented in Table 2. The reduction in water vapour from the 6-hour to the 24-hour ERA40 forecasts explain in part the

Table 2. Global-mean and low-latitude (40°S–40°N) ocean mean column-integrated water vapour and clear-sky radiation (1979–2001)

Dataset/Domain	CWV (mm)	SNLc (Wm^{-2})	OLRc (Wm^{-2})
Global			
ERA40 6-hour forecast	24.9	−81.6	264.8
ERA40 24-hour forecast	24.5	−82.1	265.2
NCEP	23.9	−85.9	268.6
Low latitude ocean			
ERA40 6-hour forecast	34.5	−75.3	283.9
ERA40 24-hour forecast	33.8	−76.2	284.3
NCEP	33.2	−79.8	287.3

reduced clear-sky net downward long-wave emission to the surface (SNLc) and increase clear-sky emission to space (OLRc), all of which result in closer agreement with NCEP data.

Evaluating the inter-annual variability and the spatial distribution of water vapour and clear-sky radiation over the 40°N–40°S ocean region it is apparent that overall, the 24-hour forecasts provide a marked improvement over the 6-hour forecasts. Further, the ERA40 24-hour forecast products show better spatio-temporal agreement with satellite observations than the other reanalysis products considered. Therefore, it is recommended that water vapour and clear-sky radiation products from the ERA40 24-hour forecasts are used in preference to other reanalysis products when considering the low-latitude ocean regions. Further assessment of water vapour and clear-sky radiation simulated by reanalyses over land is required using ground-based and satellite measurements. Agreement between both ERA40 products and NCEP are good over land regions suggesting that the spurious variability found in ERA40 6-hour forecast data is confined to the ocean and indeed relates to changes in the assimilation of satellite data over the ocean as suggested by (Uppala et al., 2005). In representing interannual variability in the atmospheric hydrological cycle in reanalyses, it may be necessary to operate a reduced but higher quality suite of observations as input to the assimilation schemes.

Acknowledgments

The input of Adrian Simmons and Igor Zveryaev is gratefully appreciated. IDL software, licensed from the Met Office, was kindly provided by Jonathan Gregory. This work was funded by the NERC grant NE/C51785X/1. The ERA40 data were retrieved from the ECMWF data services; the NCEP data were downloaded from the NOAA-CIRES Climate Diagnostics Center; the SMMR data were extracted from the Jet Propulsion Laboratory DAAC; the SRB, ERBS and CERES data were retrieved from the NASA Langley DAAC; the SSM/I data were retrieved from http://www.ssmi.com; the ScaRaB data were provided by the Centre Spatial de Toulouse; the da Silva climatology was acquired from the International Research Institute for Climate and Society LDEO Climate Data Library; and the HadISST data were kindly supplied by Nick Rayner. The comments and suggestions of two reviewers contributed substantially to the improvement of the manuscript.

References

Allan, R. P. 2006. Variability in clear-sky longwave radiative cooling of the atmosphere. *J. Geophys. Res.*, **111**, D22105. doi:10.1029/2006JD007304

Allan, R. P. and Ringer, M. A. 2003. Inconsistencies between satellite estimates of longwave cloud forcing and dynamical fields from reanalyses. *Geophys. Res. Lett.*, **30**, 1491. doi:10.1029/2003GL017019

Allan, R. P., Ringer, M. A. and Slingo, A. 2003. Evaluation of moisture in the Hadley Centre climate model using simulations of HIRS water-vapour channel radiances. *Quart. J. Roy. Meteorol. Soc.*, **129**, 3371–3389.

Allan, R. P., Ringer, M. A., Pamment, J. A. and Slingo, A. 2004. Simulation of the Earth's radiation budget by the European Centre for Medium Range Weather Forecasts 40-year reanalysis (ERA40). *J. Geophys. Res.*, **109**, D05105. doi:10.1029/2004JD005232

da Silva, A., Young, A. C. and Levitus, S. 1994. Atlas of surface marine data 1994 Volume 1: Algorithms and Procedures. Technical Report 6, NESDIS, U.S. Department of Commerce, Washington, D.C.

Huang, X., Ramaswamy, V. and Schwarzkopf, D. 2006. Quantification of the source of errors in AM2 simulated tropical clear-sky outgoing longwave radiation. *J. Geophys. Res.*, **111**, D14107. doi:10.1029/2005JD006576

Kalnay, E., Kanamitsu, M., Kistler, R., Collins, W., Deaven, and co-authors. 1996. The NCEP/NCAR 40-year reanalysis project. *Bull. Amer. Met. Soc.*, **77**, 437–471.

Prata, A. J. 1996. A new longwave formula for estimating downwelling clear sky radiation at the surface. *Quart. J. Roy. Meteorol. Soc.*, **122**, 1127–1151.

Rayner, N. A., Parker, D., Horton, E., Folland, C., Alexander and co-authors. 2003. Global analysis of sst, sea ice and night marine air temperature since the late nineteenth century. *J. Geophys. Res.*, **108**, 4407. doi:10.1029/2002JD002670

Stackhouse, P. W. J., Cox, S. J., Gupta, S. K., Dipasquale, R. C. and Brown, D. E. 1999. The WCRP/GEWEX Surface Radiation Budget Project Release 2: first results at 1 degree resolution. 10th Conf. on Atmospheric Radiation, Madison, WI. Amer. Meteor. Soc.

Stephens, G. L., Slingo, A., Webb, M. J., Minnett, P. J., Daum and co-authors. 1994. Observations of the earth's radiation budget in relation to atmospheric hydrology 4. Atmospheric column radiative cooling over the world's oceans. *J. Geophys. Res.*, **99**, 18585–18604.

Trenberth, K. E., Fasullo, J. and Smith, L. 2005. Trends and variability in column-integrated atmospheric water vapor. *Climate Dynamics*, **24**, 741–758.

Uppala, S. M., Kallberg, P. W., Simmons, A. J., Andrae, U., da Costa Bechtold, V. and co-authors. 2005. The ERA-40 re-analysis. *Quart. J. Roy. Meteorol. Soc.*, **131**, 2961–3012.

Wentz, F. J. 1997. A well-calibrated ocean algorithm for SMM/I. *J. Geophys. Res.*, **102**(C4), 8703–8718.

Wentz, F. J. and Francis, E. A. 1992. Nimbus-7 SMMR ocean products, 1979–1984. Technical report, Remote Sensing Systems Tech. Rep. 033192, 36 pp, Available at Remote Sensing Systems, College Ave., Santa Rosa, CA.

Wielicki, B. A., Wong, T., Allan, R. P., Slingo, A., Kiehl and co-authors. 2002. Evidence for large decadal variability in the tropical mean radiative energy budget. *Science*, **295**, 841–844.

Yang, H. and Tung, K. K. 1998. Water vapor, surface temperature, and the greenhouse effect—a statistical analysis of tropical-mean data. *J. Climate*, **11**, 2686–2697.

Yang, S., Hou, Y. T., Miller, A. J. and Campana, K. A. 1999. Evaluation of the Earth Radiation Budget in the NCEP-NCAR Reanalysis with ERBE. *J. Climate*, **12**, 477–493.